Understanding the impact of sub-grid scale physics in HWRF on the predicted inner-core structure and intensity of tropical cyclones

Ping Zhu, Zhenduo Zhu
Department of Earth & Environment
Florida International University

Sundararaman Gopalakrishnan, Robert Black, Frank Marks
Hurricane Research Division, AOML, NOAA

Vijay Tallapragada
Environmental Modeling Center, NCEP, NOAA

Jun Zhang, Xujing Zhang
CIMAS, University of Miami

Understanding the physical processes governing eyewall replacement cycle (ERC) in HWRF simulations.

Outline

- Impact of sub-grid scales processes on ERC in HWRF idealized simulations.
- Why operational HWRF fails to produce ERC?
- Key microphysical parameters affecting ERC in HWRF simulations.
- ERC in HWRF real case simulations

ERC in HWRF idealized simulations

Motivation

1. To what extent can model physics affect the simulation of ERC in HWRF?

2. Whether HWRF can reproduce the main characteristics of ERC simulated by WRF-ARW published recently in Zhu and Zhu (2014 and 2105) if the same initial condition and model physics are used?

3. Can HWRF with the operational model physics produce the similar result?

Initial vortex

1. An axisymmetric Cat-1 vortex with Vmax of 36.0 ms^{-1} at the radius of 45.0 km embedded in a quiescent background whose temperature and humidity profiles are specified by the non-SAL sounding of Dunion and Marron [2008].
2. Tangential wind profile at the surface is determined parametrically based on the Wood and White [2011]'s formula.
3. The surface profile is then extended into the vertical using an analytic function proposed by Nolan and Montgomery [2002].
4. The pressure and temperature fields that hold the vortex wind field are in hydrostatic and gradient wind balance, which are derived following Nolan and Montgomery [2002].
5. A water surface with a uniform temperature of 29 ^{0}C is set on an f-plane with a constant Coriolis parameter with a value equivalent to that at 20^{0}N.

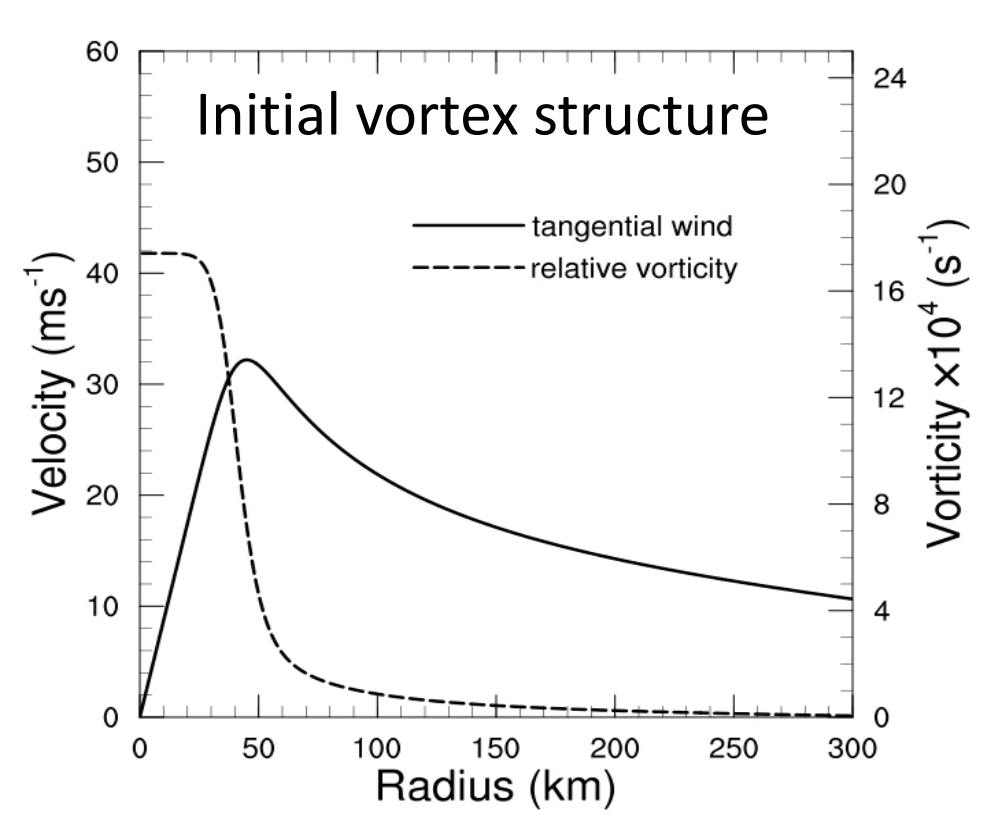

Configuration of HWRF

HWRF v3.6a

HWRF operational triple nests, $0.18^0/0.06^0/0.02^0$; 47 vertical levels; performed in the HWRF real case simulation framework.

HWRF1: HWRF operational model physics: modified Eta microphysics; modified GFDL radiation; simplified Arakawa-Schubert cumulus (outmost domain); modified GFDL surface layer scheme; and modified NCEP GFS PBL.

HWRF2: Thompson microphysics; RRTM(LW)/Dudhia(SW) radiation; Kain-Fritch cumulus (outmost domain); modified GFDL surface layer scheme; and modified NCEP GFS PBL.

10-day simulation.

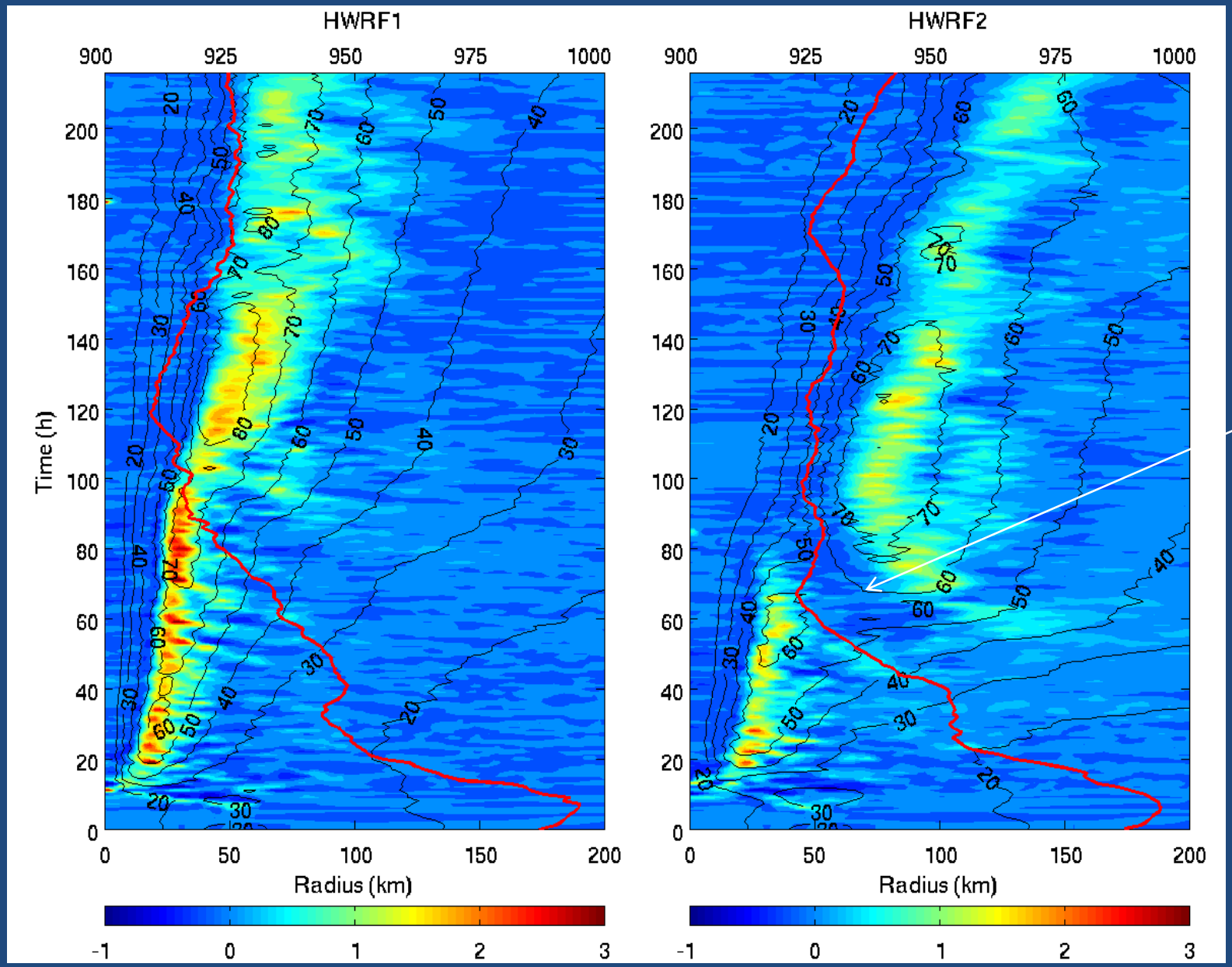

Vertical velocity at 5 km (m/s, color shades); tangential wind at 1 km (m/s, black contours); minimum sea-level pressure (MSLP, hPa, red curve scaled to the upper axis)

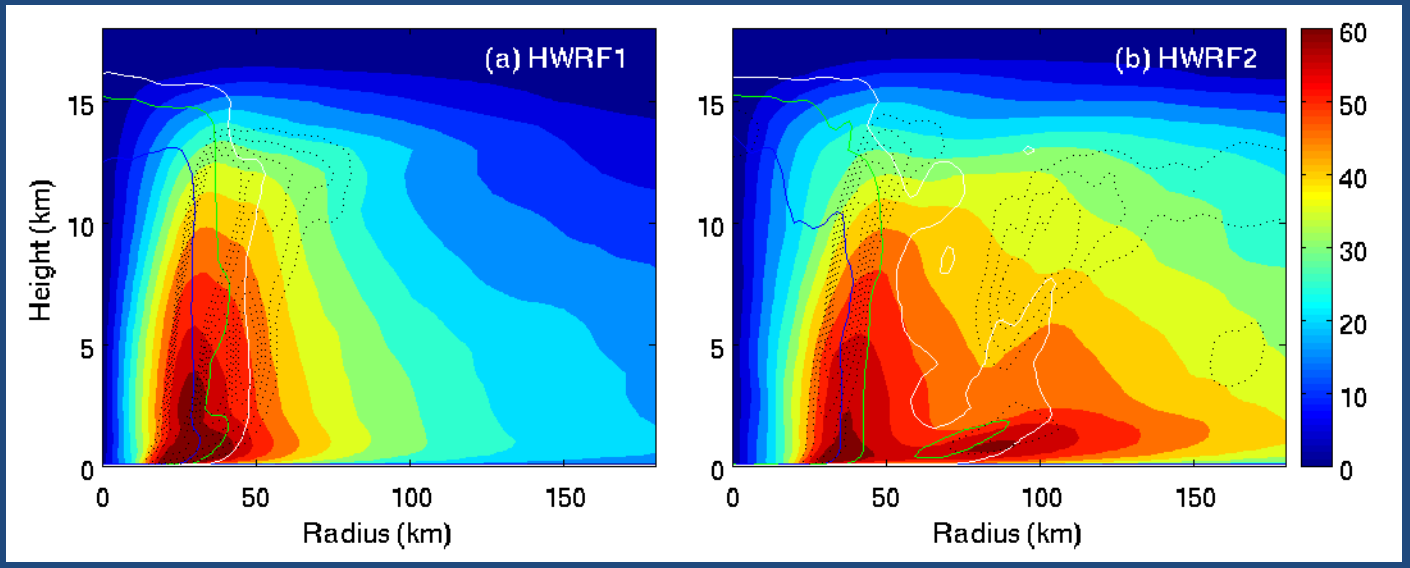

Azimuthal-mean tangential wind (color shades, ms^{-1}), relative vorticity (white, green, blue: $0.5x10^{-3}$, $1.0x10^{-3}$, $2.0x10^{-3}$ s^{-1}), updrafts (dotted black: 0.3, 0.5, 0.7, 0.9, 1.1 ms^{-1}) at the 66th h.

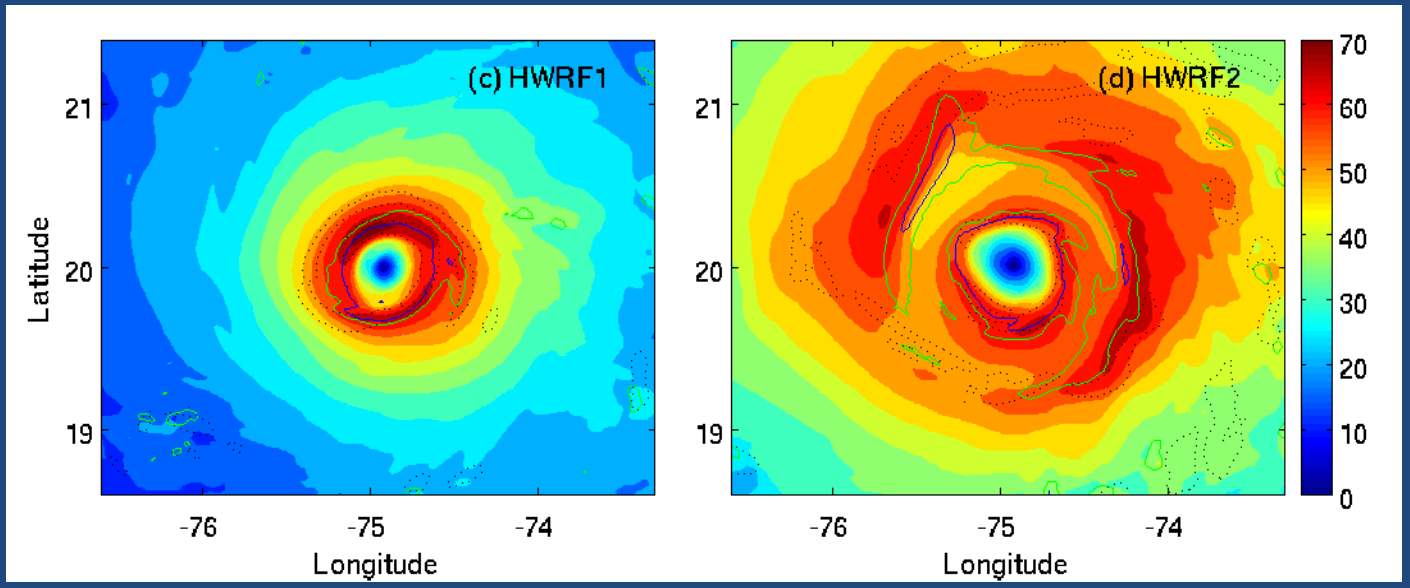

Tangential wind at 1 km (color shades, ms^{-1}), relative vorticity at 1 km (green, blue : $1.0x10^{-3}$ s^{-1}, $2.00x10^{-3}$ s^{-1}), updraft at 5 km (dotted black: 1.0 ms^{-1}) at the 66th h.

Vertical velocity (m/s) at different heights at the 66th h

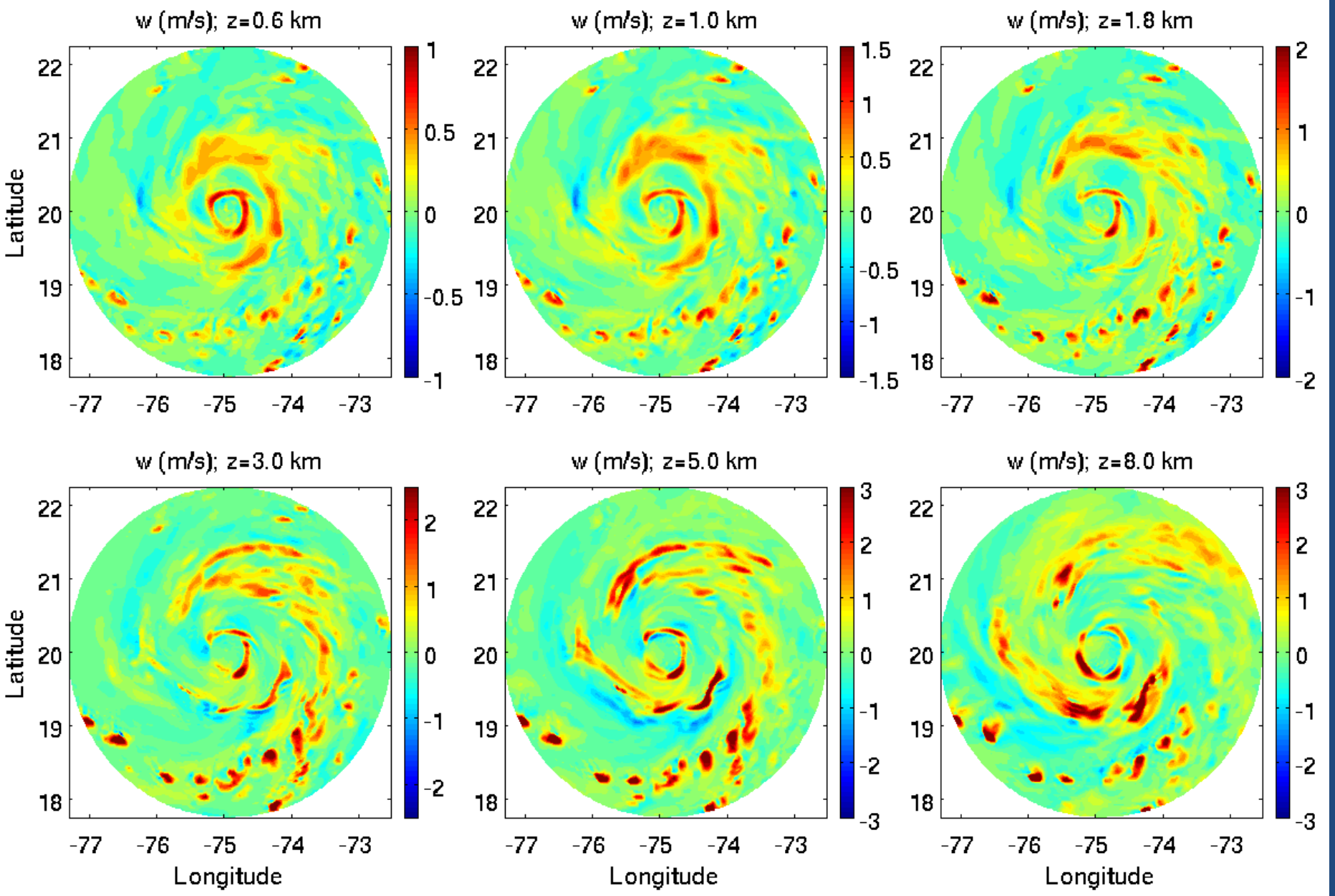

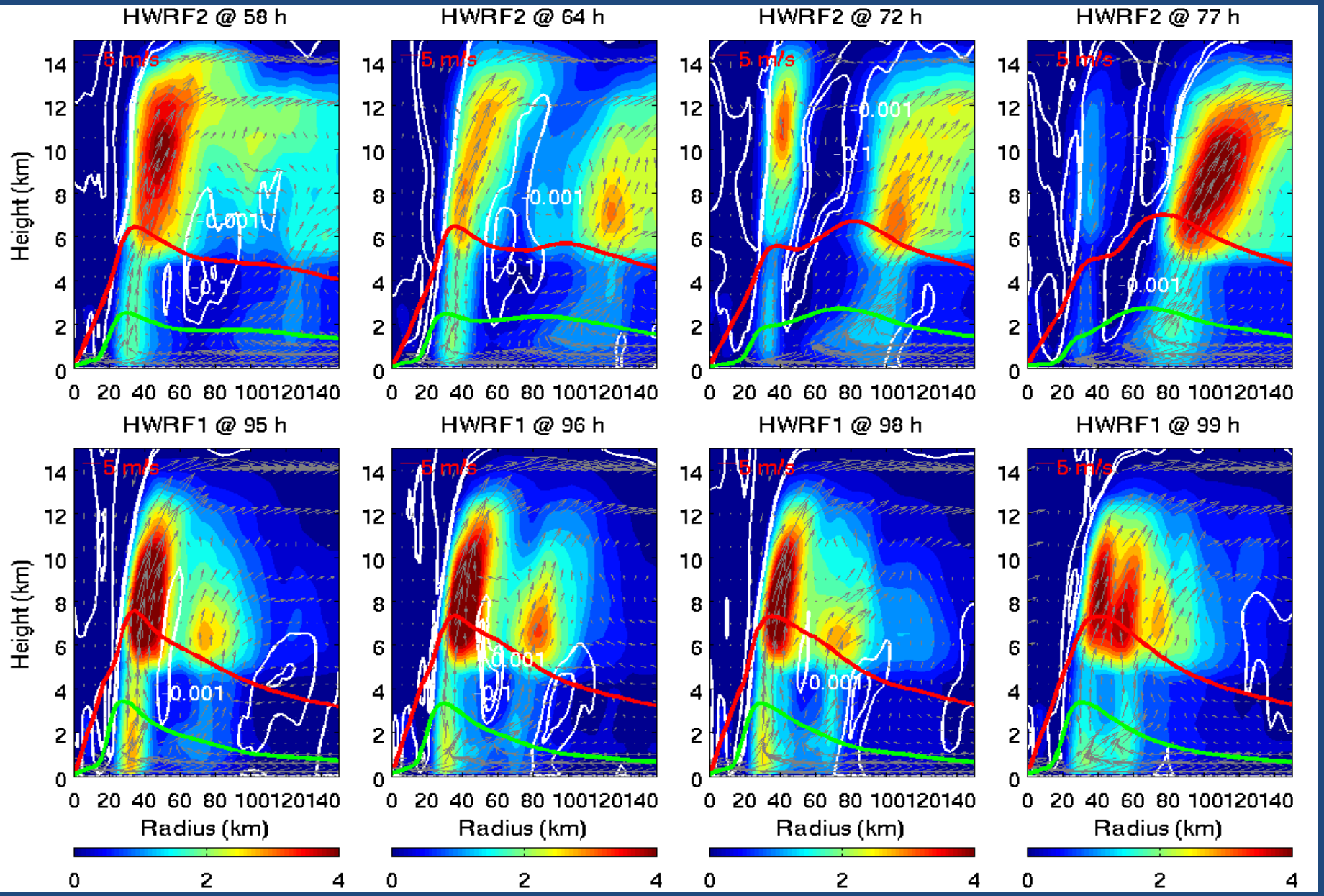

Hydrometeor mixing ratio (color shades, gkg^{-1}), downdraft (white: -0.001, -0.1 ms^{-1}), transverse circulations (arrows) during the ERC in HWRF2 and a convection episode in HWRF1. Thick red: 1 km tangential wind/10 (ms^{-1}). Thick green: surface buoyancy fluxes/100 (Wm^{-2}).

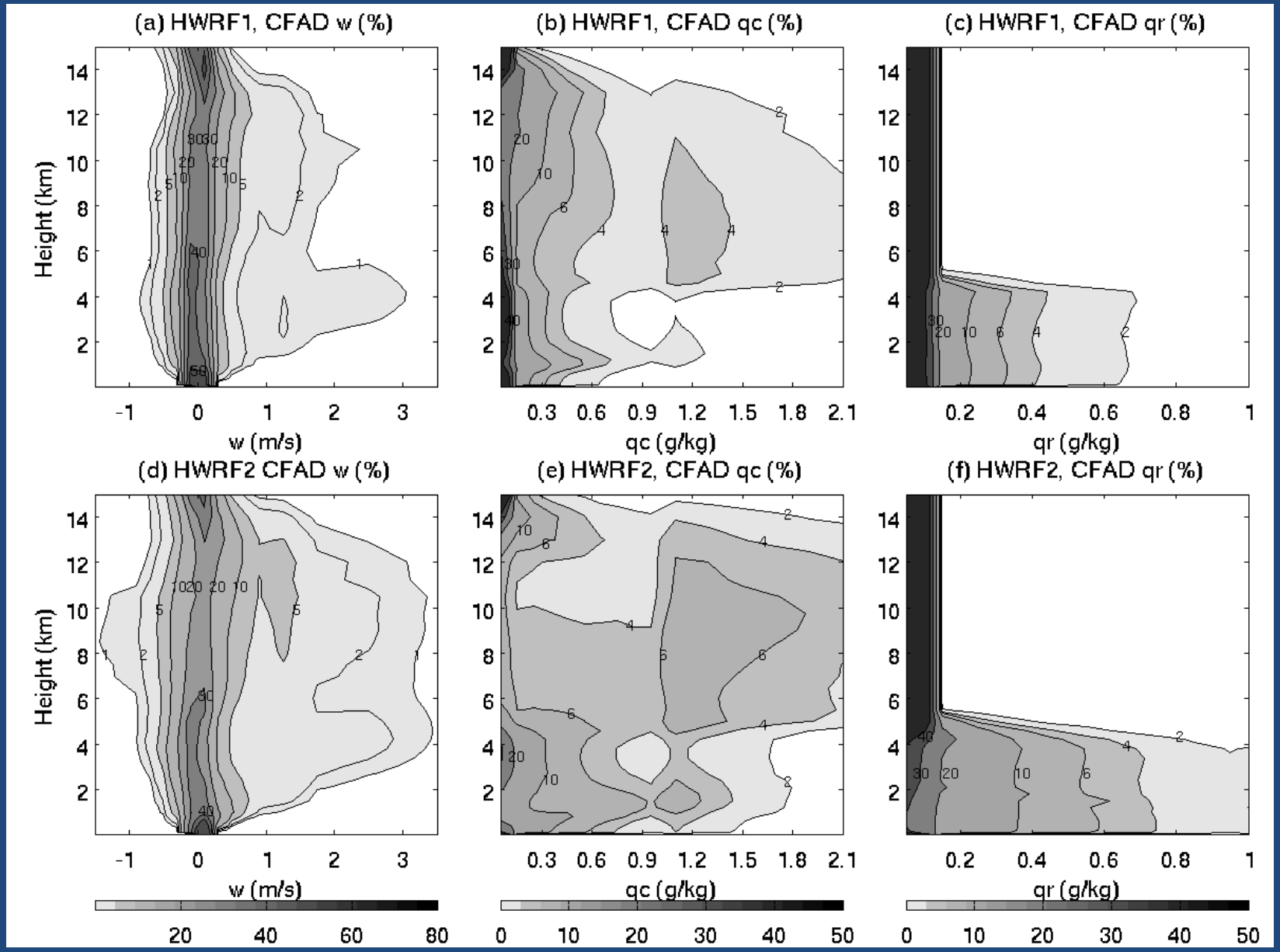

CFAD (%) of vertical velocity (w); total hydrometeor mixing ratio (q_c); rain water mixing ratio (q_r) from HWRF1 and HWRF2 in the outer rainband region (50-200 km in radius) averaged over the period from the 21st to 68th h, a period before and during the ERC of HWRF2.

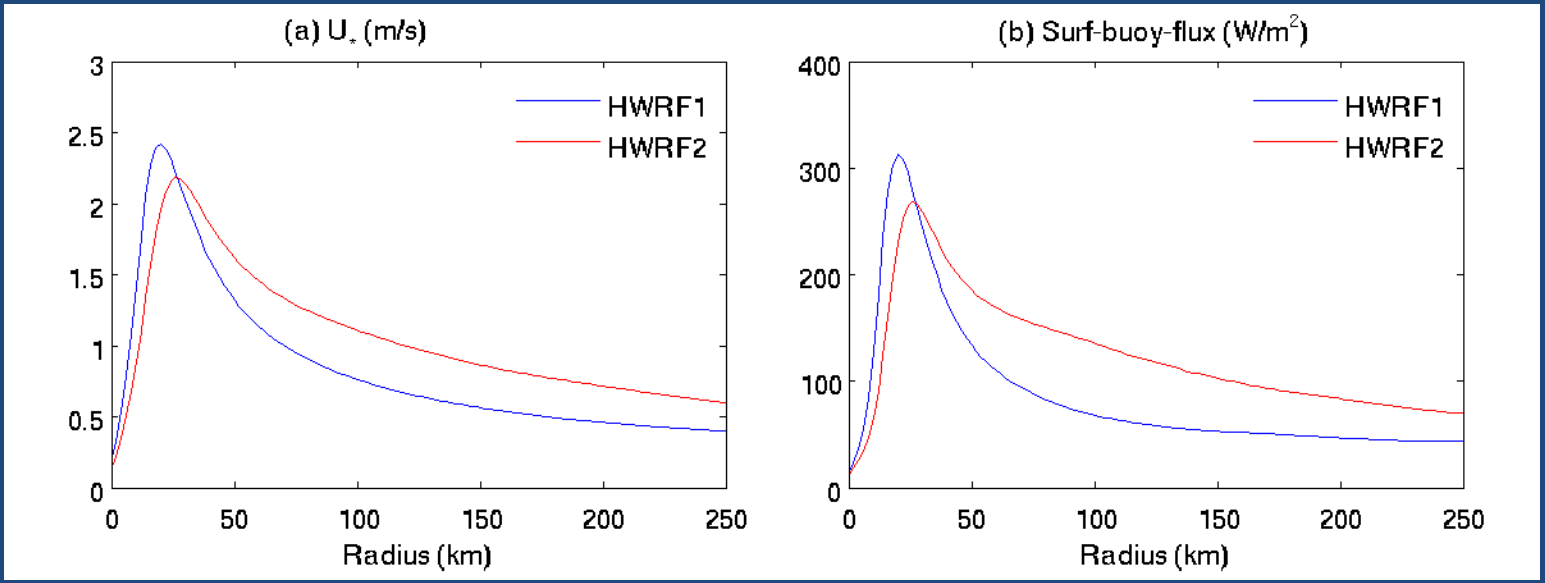

Radial profiles of friction velocity and surface buoyancy fluxes from HWRF1 and HWRF2.

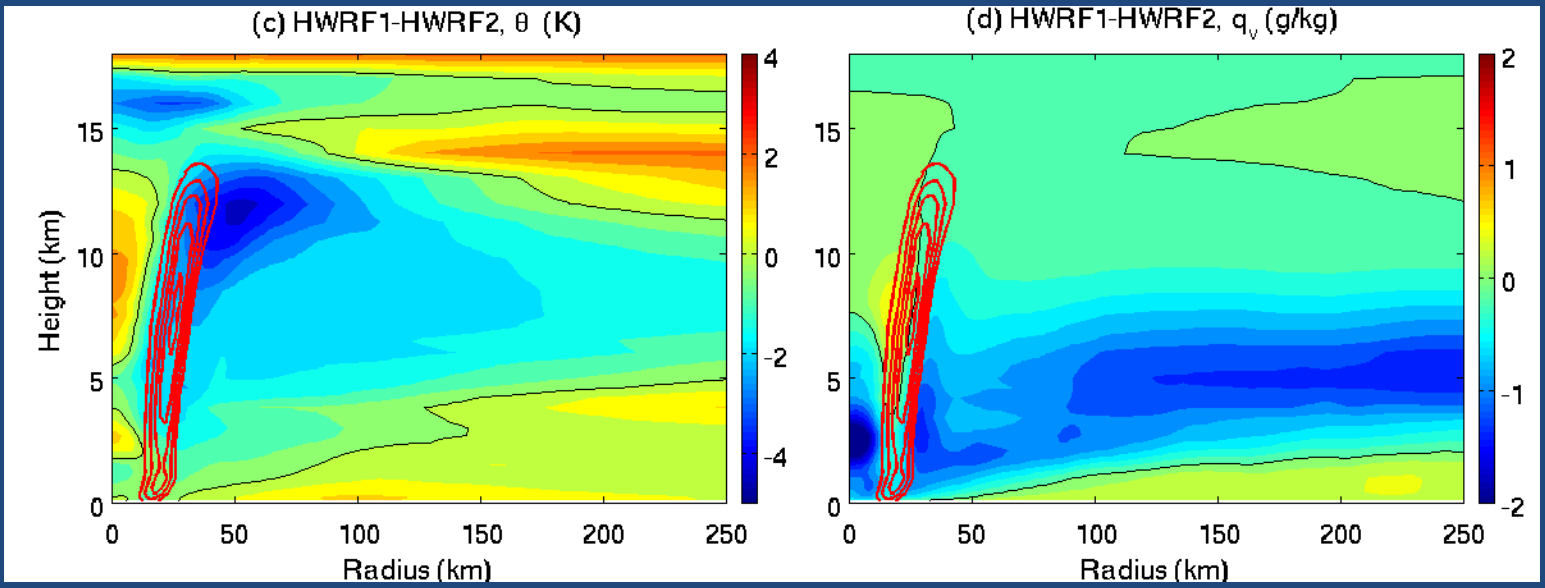

Color shades: Difference of azimuthal-mean potential temperature (θ, K) and water vapor mixing ratio (q_v, gkg^{-1}); Red contours: difference in eyewall updrafts (0.2, 0.4, 0.6, 0.8, and 1.0 ms^{-1}) between HWRF1 and HWRF2. Black: zeros. Averaged over the period from 21st to 68th h.

HWRF1 and HWRF2 involve changes in three major physics parameterizations, microphysics, radiation, and cumulus scheme. It is, thus, unclear if the resultant difference between HWRF1 and HWRF2 is due mainly to the change in specific parts of individual schemes or the combined effect of changes in all three schemes.

Can operational HWRF produce ERC by changing model physics?

Key microphysical parameters affecting ERC in HWRF simulations.

Sensitivity on snow terminal velocity and number of concentration of cloud droplet

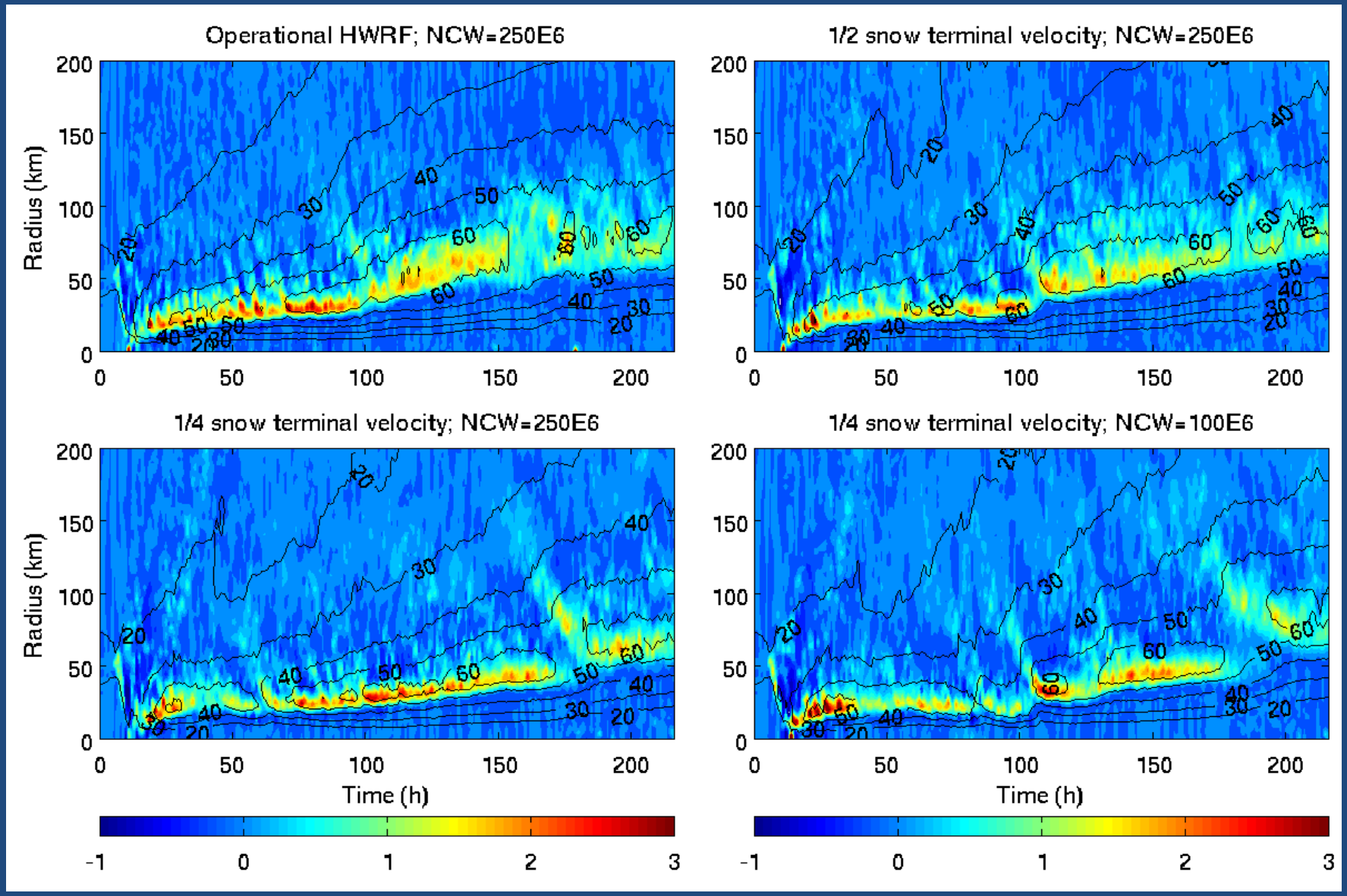

Vertical velocity at 5 km (m/s, color shades); tangential wind at 1 km (m/s, black contours) in numerical experiments with different values of STV and NCW

¼ STV; NCW=100E6 at 177th h

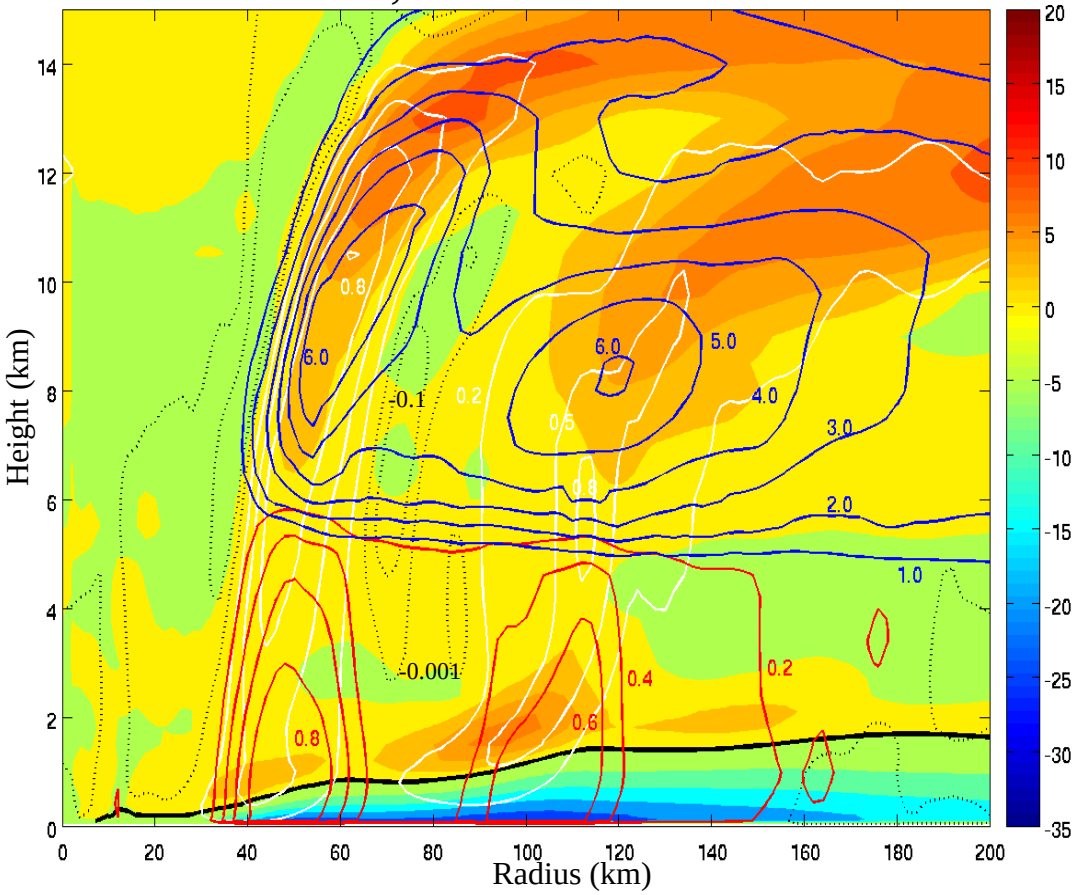

Operational HWRF at 177th h

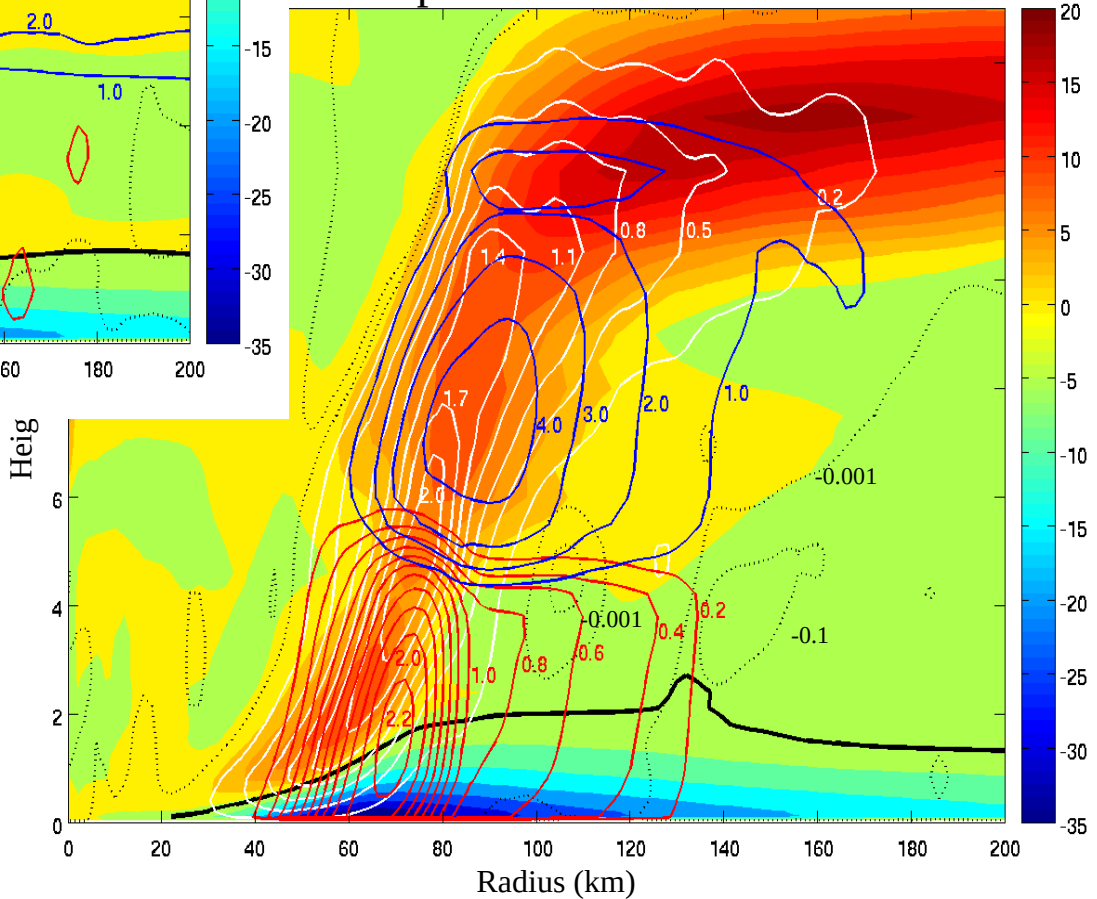

Radial velocity (m/s, color shades; black: zero); updraft (m/s, white contours); downdraft (m/s, dotted black); solid hydrometeor mixing ratio (g/kg, blue contours); rain water mixing ratio (g/kg, red contours) in experiments with HWRF operational microphysics and with ¼ STV and NCW=100E6.

The idealized simulations show that the ice-phase microphysics and precipitation parameterization can have a profound impact on the processes governing SEF and ERC. However, the idealized simulation itself cannot answer if ERC should be or should not be generated for this particular initial setting of vortex.

ERC in Hurricane Rita (2005)

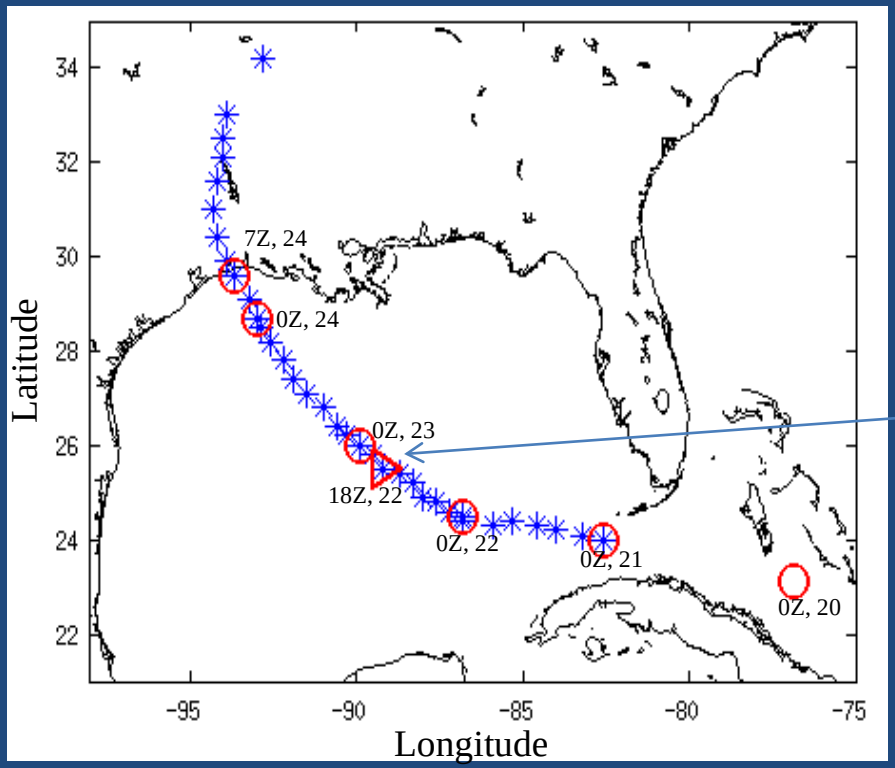

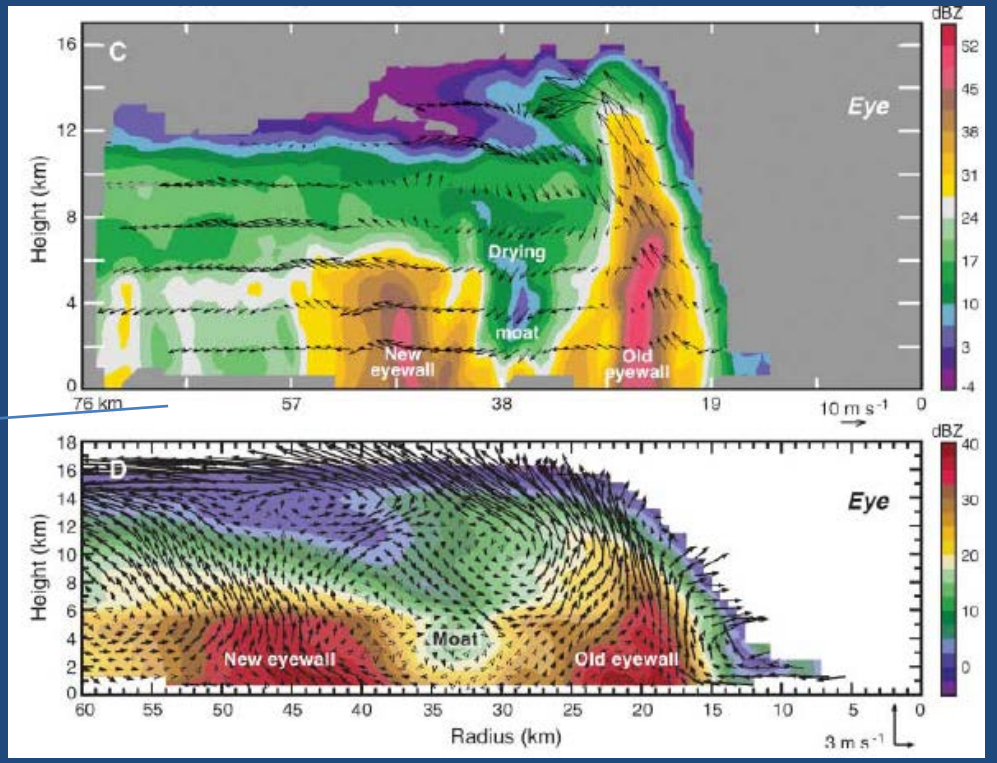

Reflectivity and transverse circulation at 1800-1820UTC, 22 Sept. (C): northwest cross-section. (D): comprehensive mean adopted from Houze et al. (2007)

ERC of Rita simulated by WRF-ARW

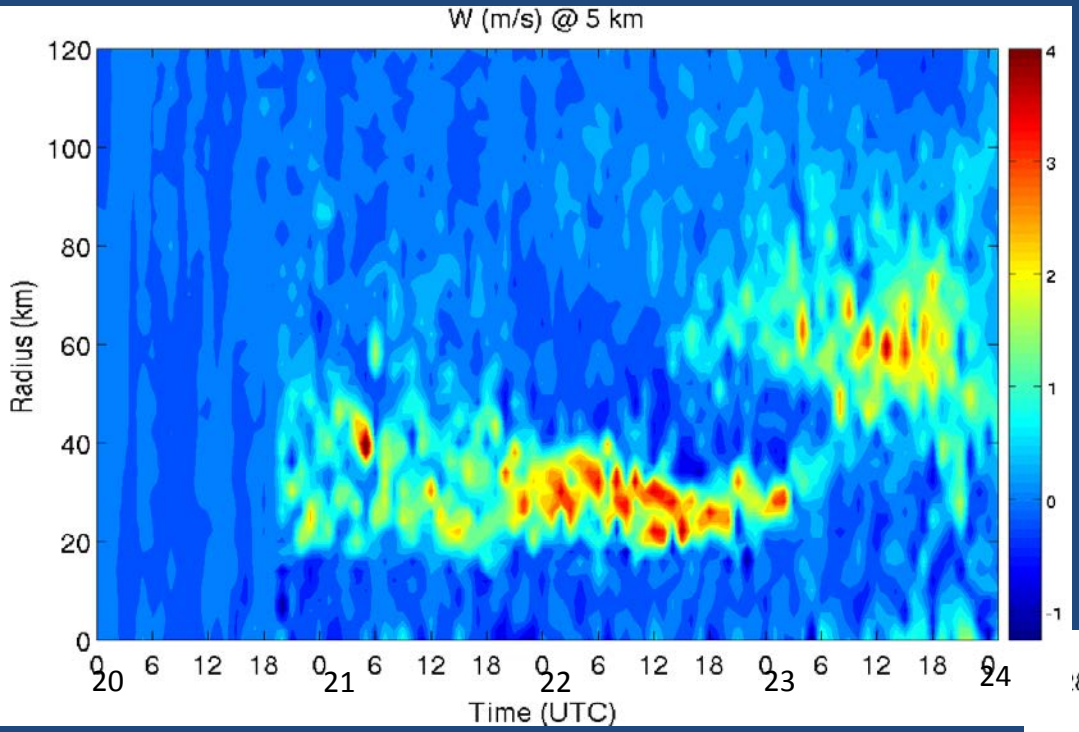

Simulation starting at 00 Z, 20 Sept.
Grid-spacing: 18/6/2 km
Grid-mesh: 310, 184, 310
Vertical level: 47
GFS data

Thompson microphysics;
RRTM(LW)/Dudhia(SW) radiation;
Kain-Fritch cumulus;
MYJ PBL and the associated surface layer parameterization.

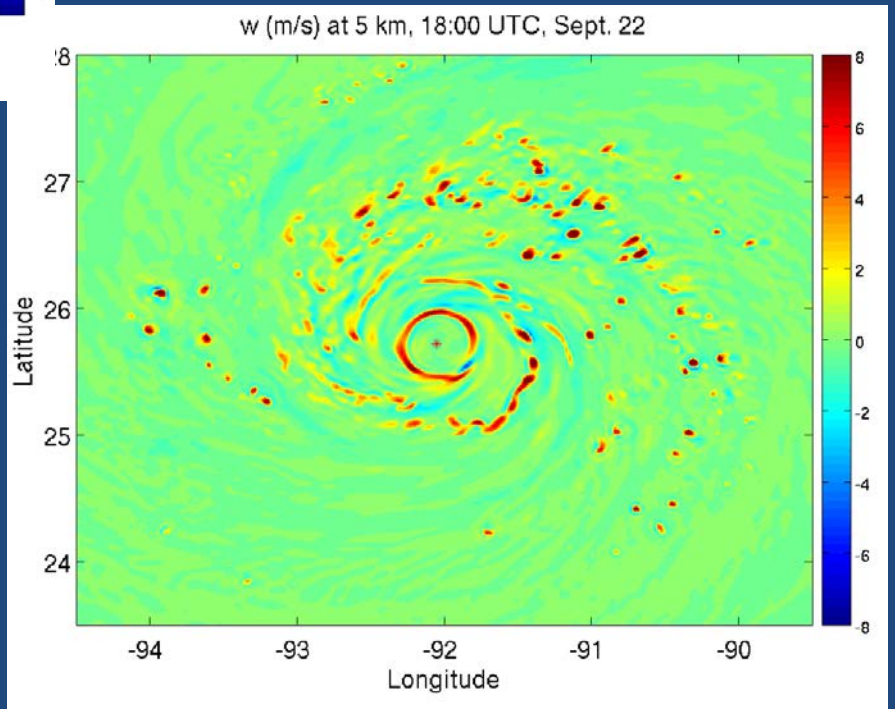

ERC of Rita simulated by HWRF

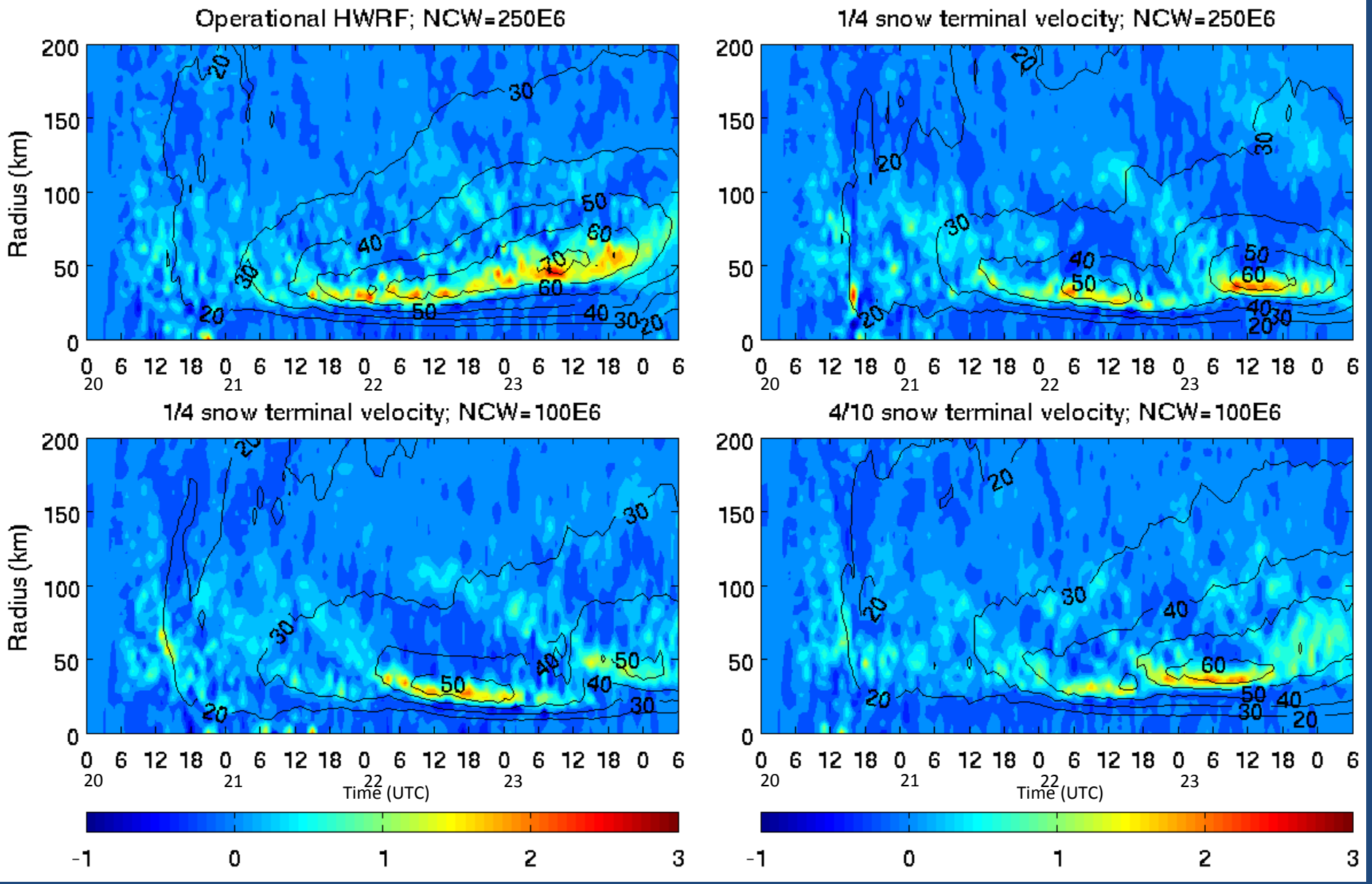

Vertical velocity at 5 km (m/s, color shades); tangential wind at 1 km (m/s, black contours) in numerical experiments with different values of STV and NCW

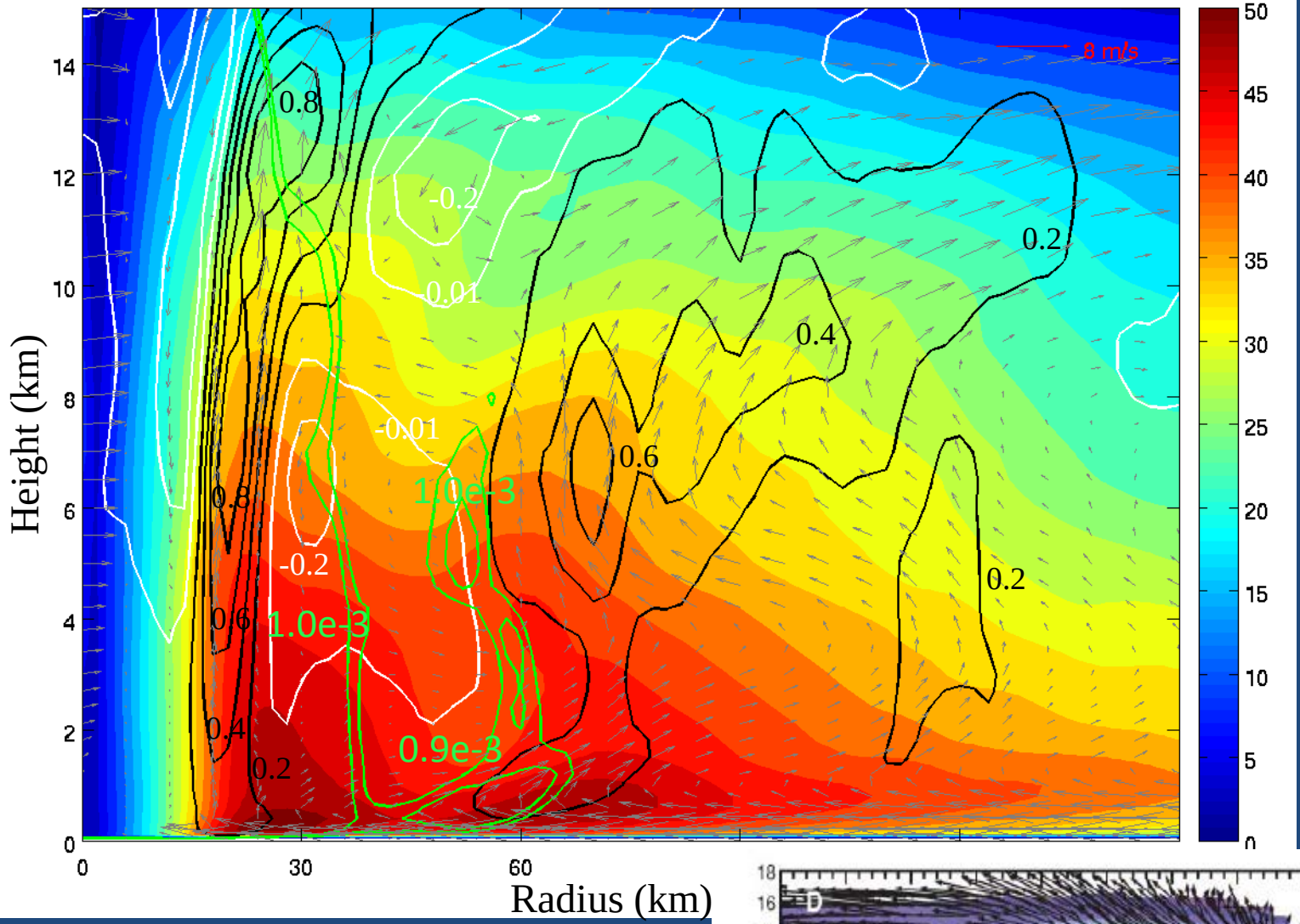

Z-R structure of Rita double eyewalls in the HWRF experiment of ¼ STV and NCW=100E6

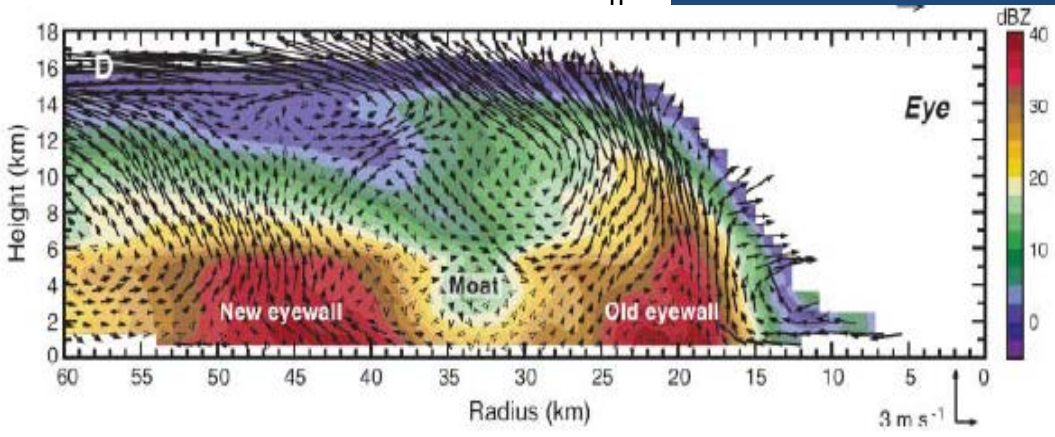

Azimuthal-mean tangential wind (color shades, ms^{-1}), relative vorticity (green, s^{-1}), updrafts (black, ms^{-1}), downdrafts (white, ms^{-1}) at 5:00 UTC 23 Sept.

Vertical velocity (m/s) at different heights at 5:00UTC 23 Sept.

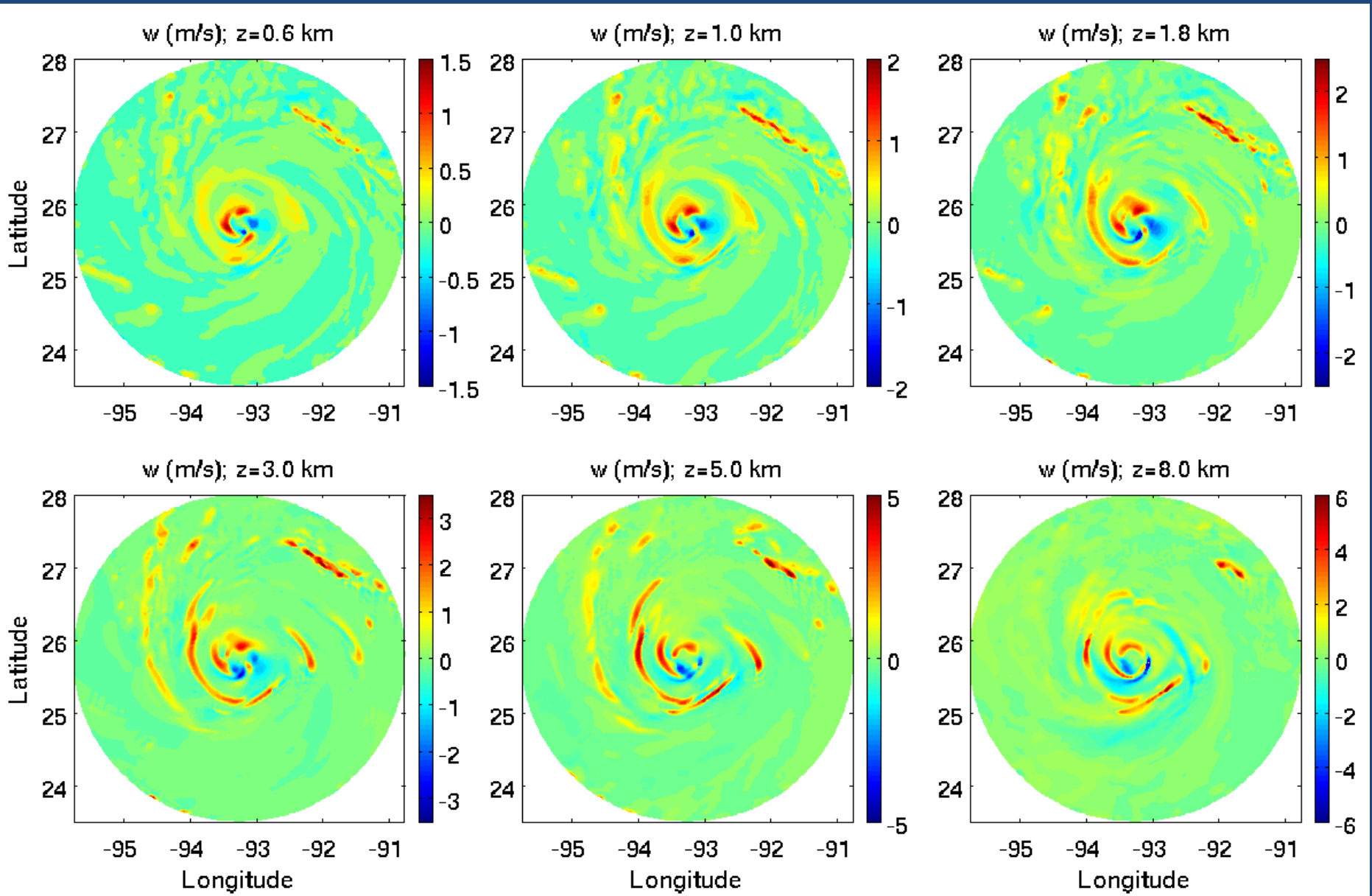

Conclusion

1. While HWRF with the operational model physics fails to produce ERC in the idealized simulation, HWRF with the Thompson microphysics, Dudhia/RRTM radiation, and Kain-Fritch cumulus, is able to generate a “clean” ERC with the formation mechanism and characteristics similar to that simulated by WRF-ARW (Zhu &Zhu 2014).

2. The failure of producing ERC by HWRF operational model physics is due to the lack of outer rainband convection at the far radii, excessive solid-phase hydrometeors in the moat region, and enhanced shallow convection, which all tend to prevent a persistent moat forming in-between eyewall and outer rainband. The less evaporative cooling from precipitation in the operational HWRF is the culprit for producing a more stable and dryer environment that inhibits the development of systematic convection at the far radii in the outer rainband region.

3. The challenge for operationally predicting ERC stems from the fact that the feedback among the processes governing ERC depends strongly on how SGS processes are parameterized and how they interact with each other and with the resolved processes. Changes in model physics are sufficient in kicking off and driving the feedback in different directions, leading the storm to evolve along a totally different pathway.

4. ERC in HWRF shows a substantial sensitivity to ice-phase microphysics and precipitation parameterization. Snow terminal velocity and number of concentration of cloud droplet pose a great impact on the occurrence and structure of concentric convection rings associated with ERC. Large snow terminal velocity causes snow to fall quickly and melt in the low level, and hence, enhances the inner eyewall diabatic heating to result in a strong radial inflow in the BL. The persistent fuel supply into the eyewall by the strengthened BL inflow leads to a long-lived eyewall. On the other hand, small snow terminal velocity and small number of concentration of cloud droplet appear to favor the development of outer rainband convection leading to the formation of concentric outer eyewall.

Remark

1. All parameterization schemes tested in this study are widely used in numerical simulations and some of them have been extensively evaluated in different conditions as individual schemes. However, the complicated sensitivity of ERC to these schemes suggests that the interaction between schemes and the feedback between resolved and parameterized processes are far from well understood.

2. The modification of STV and NCW in our experiments is only for the purpose of demonstrating the importance of microphysics to ERC simulations in HWRF. It should not be interpreted as a way of tuning parameterizations. However, it suggests that ice-phase microphysics and autoconversion/accretion parameterization need to be further evaluated.